# Signal-to-Noise Ratio Comparison Between Surface Coils and Implanted Coils

Lance L. Arnder, Mark D. Shattuck, Robert D. Black

**The signal-to-noise ratio (SNR) from implanted coils is widely known to be superior to that from surface coils. This article addresses the quantitative aspects of this improvement by explicitly evaluating the magnetic vector potential in a conducting medium of finite extent for both implanted and surface coils. The predictions of the model are tested with actual image data from spin warp experiments on gelatin phantoms. The authors derived a simplified expression that yields the gain in SNR of an implanted coil relative to that of a surface coil and is valid in many practical situations.**

**Key words: signal-to-noise (SNR); implanted coils; surface coils; magnetic resonance microscopy.**

## INTRODUCTION

A fundamental problem in MR microscopy is how best to image a structure of interest at a distance from the surface of a specimen. Often, it is desirable to limit the field of view so as to avoid extraneous noise and unwanted signal from neighboring regions. The signal-to-noise ratio (SNR) advantage of a surface coil over that of a volume coil for structures near the surface of a specimen is well known (1). Explained most simply, a surface coil consists of a loop of wire and a matching network that is necessary to maximize power transfer from the loop to the preamplifier. Inductively coupling to a resonant loop (the surface coil) with a pickup loop is a convenient matching technique. Inductive coupling is distinct from other coupling techniques (2) in that the resonating loop on the surface of the specimen is physically separate from the pickup loop. This distinction can be used to good advantage for *in vivo* studies allowing the surgical implantation of the resonating loop (see refs. 3, 4) (Fig. 1).

Several recent studies have demonstrated the feasibility of using implanted coils for *in vivo* imaging with in-plane resolutions as fine as 25 $\mu$m (3, 5–7). In this article, expressions are developed for both the signal and noise voltages available to the preamplifier for both surface coil and implanted coil imaging systems. A comparison is made between the SNRs (per voxel) of these systems, and the predictions are empirically verified.

**MRM 35:727–733 (1996)**

From the Department of Radiology (L.L.A.), University of North Carolina, Chapel Hill; Center for *In Vivo* Microscopy, Departments of Physics (M.D.S.) and Radiology and Biomedical Engineering (R.D.B.), Duke University, Durham, North Carolina.

Address correspondence to: Elaine G. Fitzsimons, M.S., Center for *In Vivo* Microscopy, Box 3302, Duke University Medical Center, Durham, NC 27710.

Received April 19, 1995; revised October 26, 1995; accepted November 30, 1995.

This work was supported by Sandoz Pharmaceuticals, NIH Grant P41-RR05959, and NSF Grant CDR-8622201.

0740-3194/96 $3.00



## THEORY

To calculate expressions for the signal and noise components for a given coil configuration, the magnetic field must be known in the region of interest. This is most easily accomplished by computing the magnetic vector potential, **A**, for all points in space. Harpen (8) provides a compact formula for the inductive losses seen by means of a coil over a conducting half-space. This treatment ignores penetration depth effects. Hammond (9) provides a more general treatment that includes eddy current effects, and his approach is adopted here, modified for a finite sample volume. An approximation is made in that the **A**-field lines are evaluated by assuming that the conducting medium fills an infinite half-space. However, integration is limited to the actual sample volume. This approximation becomes better at higher frequencies and for implanted coils that are small, compared to the planar extent of the sample. We now introduce some preliminary terms and derive expressions for the signal and noise components for a given coil configuration.

The following definitions will facilitate discussion: implanted coil, the implanted resonant structure; pickup coil, that part of the implanted coil system that lies on or near the surface of the specimen and inductively couples to the implanted coil; surface coil, an imaging coil that lies entirely on the surface of the specimen. The terms "pickup" and "implanted" will be used instead of "secondary" and "primary," when referencing coils for clarity, although the latter terms emphasize that the discussion applies to other inductively coupled systems and that the two-coil system acts simply as a transformer.

To calculate the SNR available to the preamplifier, or the system SNR, all signal and noise sources must be referred to the preamplifier. It is equivalent, however, to calculate the SNR in the pickup/surface coil, because the matching network is assumed to be a purely reactive, lossless, linear network. That is, the SNR in the pickup or surface coil is the SNR available to the preamplifier, because both signal and noise are transformed, or referred, across the matching network equivalently. It is important to remember to refer the noise of the preamplifier into the pickup or surface coil when calculating the SNR in this stage. Finding the SNR in the implanted coil is not equivalent to calculating the SNR at the preamplifier, because the network between the implanted coil and the preamplifier is, in general, lossy. The following definitions can now be made:

$R_i$, $R_p$, $R_s$, and $R_{pre}$ are the nominal resistances, or resistances in isolation, of the implanted coil, pickup coil, surface coil, and preamplifier, respectively.

$R_{it}$ is the total resistance of the implanted coil, including the coupled resistance of the pickup coil circuit and preamplifier.

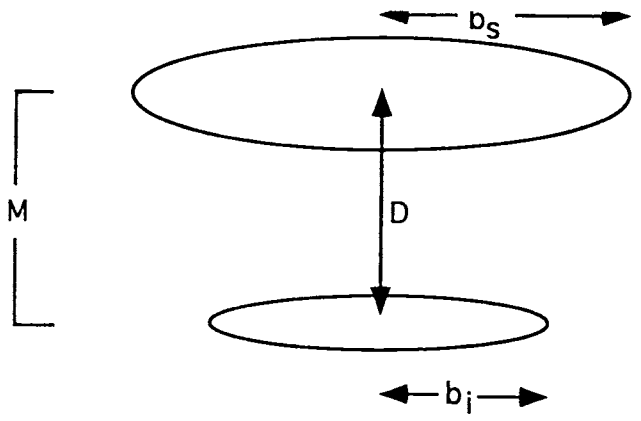


FIG. 1. The surface ($b_s$) or secondary coil and the implanted ($b_i$) or primary coil. M = mutual inductance.

$R_{pt}$ is the total resistance of the pickup coil, including the coupled resistance of the implanted coil and the referred resistance of the preamplifier.
$R_{st}$ is the total resistance of the surface coil, including the referred resistance of the preamplifier.

The subscript notation introduced here will be used throughout the remainder of the article. That is, variables associated with the implanted coil, pickup coil, surface coil, and preamplifier will be subscripted with *i, p, s,* and *pre-*, respectively. A resistance or impedance with a subscript ending in *t* will denote a total resistance or impedance that includes all other referred resistances or impedances, respectively.

Central to an understanding of how to analyze inductively coupled circuits are the following rules (2):

$$emf_p = -j\omega_0 m I_i = -j\omega_0 m \frac{emf_i}{R_{it}} \quad [1]$$

$$Z_{i\to p} = (\omega m)^2 / Z_i, \quad [2]$$

where $emf_p$ is the voltage induced in the pickup coil due to a current, $I_i$, flowing in the implanted coil, $emf_i$ is the nuclear magnetic resonance voltage induced in the implanted coil, $m$ is the mutual inductance between two coils, $Z_{i\to p}$ is the impedance coupled, or referred, into the pickup coil from the implanted coil.

The influence of the pickup coil on the implanted coil can be determined from these equations by simply exchanging subscripts. The reader may find it helpful to read the arrow in the subscript notation as "referred."

It can be shown that, because the matching network is lossless, linear, and transforms $R_{i\to p} + R_p$ to the impedance of the preamplifier, the converse is true, i.e., the preamplifier resistance transforms back across the matching network as $R_{i\to p} + R_p$. The following expressions can now be provided. These expressions assume that the implanted and pickup coils are resonant, i.e., that the impedances of these coils are purely resistive:

$$R_{i\to p} = (\omega_0 m)^2 / R_i \quad [3]$$

$$R_{pre\to s} = R_s \quad [4]$$

$$R_{pre\to p} = R_p + (\omega_0 m)^2 / R_i \quad [5]$$

$$R_{pt} = R_p + R_{i\to p} + R_{pre\to p} = 2(R_p + R_{i\to p}) = 2[R_p + (\omega_0 m)^2 / R_i] \quad [6]$$

$$R_{it} = R_i + (R_p + R_{pre\to p})_{\to i} = R_i + \frac{(\omega_0 m)^2}{2R_p + (\omega_0 m)^2 / R_i} \quad [7]$$

$$R_{st} = R_s + R_{pre\to s} = 2R_s. \quad [8]$$

For the purposes of this discussion, SNRs will be developed for a voxel *v* with volume, *V*, and a distance, *D*, from the surface of the specimen/sample, which is taken to be a cylinder of tissue below the surface coil or pickup coil. It is also assumed that the tissue within the voxel is uniformly excited, so that the magnetization vector, **M**, is rotating in the transverse plane at the end of excitation (90° tip angle). The surface coil is assumed to be a single turn loop of radius $b_s$ with its axis perpendicular to $\mathbf{B_0}$. Similarly, the pickup and implanted coils are assumed to be single-turn loops of radii $b_p$ and $b_i$, respectively. The axes of the pickup and implanted coils are assumed to be collinear, and the implanted coil is assumed to lie a distance, *D*, below the surface of the specimen. The voxel is assumed to lie along the axes of all coils, which is taken to be the *y* axis.

## Signal Developed in a Coil

To derive signal and noise expressions, the vector potential field, **A**, and the magnetic field, **B**, arising from a current flowing in a circular coil (antenna) must be known. In conductive media, the magnitude of these fields will be smaller than in free space due to eddy current shielding. Analytical solutions for these fields, including the effect of eddy current shielding, exist when conductive media are a half-space at or below the circular coil when the axis of the coil is normal to the half-space (9). When conductive media are finite in extent, analytical solutions exist only for specific sample and coil geometries although, in general, Maxwell's equations can be solved numerically, using the boundary conditions associated with the particular situation. As mentioned previously, the actual fields are approximated with the analytical solutions obtained, assuming an infinite half-space of conductive media.

The signal or *emf* induced in a coil from *v* is as follows (10):

$$emf = \frac{-\partial}{\partial t}[\mathbf{B_1}/I \cdot \mathbf{M}]. \quad [9]$$

where $\mathbf{B_1}/I$ is the magnetic field developed by unit current in the coil and **M** is the net nuclear magnetization vector after excitation at *v*.

Because $\mathbf{B_1}$ at *v* lies along the *y* axis, and $\mathbf{B_1}/I$ does not vary with time:

$$emf = -B_1 \Big/ I \frac{\partial}{\partial t} M_y. \quad [10]$$

Immediately after excitation, assuming that transmit power has been adjusted so that a tip angle is achieved at $v$, $\mathbf{M}$ is a vector rotating in the $x$-$y$ plane at the Larmor frequency and, therefore, $M_y = M_0 V \sin(\omega_0 t + \phi)$, where $M_0$ is the maximum magnetization per unit volume, $\phi$ is an arbitrary phase angle, and $\omega_0$ is the Larmor frequency corresponding to the static magnetic field strength, $B_0$. It follows that:

$$emf = (-B_1/I)\omega_0 M_0 V \cos(\omega_0 t + \phi) \quad [11]$$

and

$$emf_{\text{rms}} = (B_1/I)\omega_0 M_0 V/\sqrt{2}. \quad [12]$$

For protons in water at 310 K, assuming a long *TR*, short *TE* experiment (11), $M_0 = 3.25 \cdot 10^{-3} B_0$ ($\text{Am}^{-1}$). The quantity in Eq. [11] that changes when one uses either a surface coil or an implanted coil is the $B_1/I$ ratio.

With an implanted coil and a pickup coil, the $B_1$ field at $v$ is the sum of $B_{1p}$ and $B_{1i}$, the fields produced by the current, $I_p$, flowing in the pickup coil, and the induced current, $I_i$, flowing in the implanted coil, respectively. For practical purposes, the $B_1$ field at $v$ is dominated by $B_{1i}$($B_{1p}$ will be neglected). Using Eq. [1], the signal that is actually measured is the voltage induced in the pickup coil, $emf_p$ (2):

$$emf_p = -j\omega_0 m I_i = -j\omega_0 m \frac{emf_i}{R_{it}} \quad [13]$$

and from Eqs. [11] and [12]

$$emf_{p,\text{rms}} = \omega_0 m \frac{(\omega_0 M_0 V B_1/I_i)}{\sqrt{2}R_{it}}. \quad [14]$$

The resistance of a coil—surface, pickup, or implanted—includes both a component resistance, $R_{\text{component}}$, a sample resistance $R_{\text{sample}}$, and a radiation resistance $R_{\text{radiation}}$, i.e., $R_{\text{coil}} = R_{\text{component}} + R_{\text{sample}} + R_{\text{radiation}}$ (see Appendix A).

Sample losses consist of both inductive or Faraday losses and dielectric or Coulomb losses. Inductive losses are assumed to dominate dielectric losses, and for the remainder of this discussion, dielectric losses will be neglected. In a subsequent section, empirical evidence will be presented that demonstrates that this assumption holds, at least at high field. General expressions for the dielectric loss are not available in the literature. $R_{\text{radiation}}$ is the apparent resistance through which power dissipates due to radiation of energy. It is important to note that although this resistance consumes power and is important for matching considerations, it is not dissipative in the sense that it generates noise (see the next section).

## Noise Developed in a Surface/Pickup Coil

A coil noise voltage $E_n$ can be developed via the fluctuation dissipation theorem in terms of $R$, the effective resistance through which power dissipates. It is well known that rms voltage noise is given by (e.g., ref. 12):

$$E_n = \sqrt{4kTR\Delta F}, \quad [15]$$

where $k$ is the Boltzmann constant, $T$ is the absolute temperature, and $\Delta F$ is the receiver bandwidth in hertz.

The total noise at a stage of a circuit, e.g., the pickup coil, can be determined by referring all impedances to that stage of the circuit for a total resistance, $R_t$, and then invoking the fluctuation dissipation theorem.

Referring resistances into a stage of a circuit to calculate noise is more convenient than using the more general technique of calculating individual noise voltages and referring these noise voltages into a stage of a circuit. When using the more general technique, the geometric mean must be used when adding two uncorrelated noise voltages, because uncorrelated rms noise voltages do not add linearly, although their corresponding powers do. The simpler technique works, in general, only if the noise temperatures of the resistances are the same. If resistance noise temperatures are not the same, the more general technique of calculating individual noise voltages is required. This allows the effects of changing the noise temperature of resistances (noise sources) on system SNR to be modeled and investigated separately from their ohmic properties and their effects on matching. For example, the noise temperature of radiation resistance is zero, and although most MRI preamplifiers have input impedances of 50Ω, their effective noise temperatures are often less than 30° K. However, the simpler technique will allow practical expressions for SNR to be developed and will be used for this derivation.

## SNR Expressions

Signal-to-noise ratios for both the surface and pickup coils can now be provided:

$$\text{SNR}_p = \frac{emf_{p,\text{rms}}}{E_{n,p}} = \frac{((\omega_0 M_0 V B_1/I_i)/\sqrt{2}R_{it})}{\omega_0 m \sqrt{4kT\Delta F R_{pt}}} = \frac{\omega_0^2 m M_0 V B_1/I_i}{\sqrt{2}R_{it}\sqrt{4kT\Delta F R_{pt}}} \quad [16]$$

$$\text{SNR}_s = \frac{emf_{s,\text{rms}}}{E_{n,s}} = \frac{\omega_0 M_0 V B_1/I_s}{\sqrt{2}\sqrt{4kT\Delta F R_{st}}} \quad [17]$$

$$\frac{\text{SNR}_p}{\text{SNR}_s} = \frac{\omega_0 m B_1/I_i}{R_{it}\, B_1/I_s}\left[\frac{R_{st}}{R_{pt}}\right]^{1/2}. \quad [18]$$

The mutual inductance between the pickup and implanted coil was provided by Smythe (13):

$$m = \int_{s_i} (\mathbf{B_1}/I_p) \cdot d\mathbf{s}_i \cong (B_1/I_p)\pi b_i^2. \quad [19]$$

Assuming that the surface and pickup coil radii are equal, $B_1/I_s = B_1/I_p$ and

$$m \cong (B_1/I_s)\pi b_i^2. \quad [20]$$

In general, the radii of the pickup and the surface coil corresponding to maximum SNR are not the same. However, for practical purposes, these optimal radii are, as will be shown in a subsequent section, equivalent. This equivalence will be assumed for the remainder of the derivation.

Approximating $B_1/I_i$ in the lossy medium with the corresponding free space formula $B_1/I_i = \mu_0/(2b_i)$ (13),

$$\frac{\mathrm{SNR}_p}{\mathrm{SNR}_s} = \frac{\omega_0\mu_0\pi b_i}{2R_{it}}\left[\frac{R_{st}}{R_{pt}}\right]^{1/2}. \qquad [21]$$

A special case of practical interest occurs when $R_{i\to p} \gg R_p$. When this condition holds, $R_{pt} \cong 2(\omega_0 m)^2/R_i, R_{it} \cong 2R_i$, and $R_{st} \cong 2R_s$. Therefore,

$$\frac{\mathrm{SNR}_p}{\mathrm{SNR}_s} \cong \frac{\mu_0\pi b_i}{4mR_i}\left[\frac{R_s}{R_i}\right]^{1/2}. \qquad [22]$$

An approximation for $R_s$and$R_i$, assuming that $R_{\mathrm{sample}}$ dominates the other resistance components, can be found using the following formula (6):

$$R_{\mathrm{sample}} \cong 0.0332g(\omega_0\mu_0\pi)^2\, a^3, \qquad [23]$$

where $a$ is the coil radius. This formula assumes no eddy current shielding of the magnetic field and an infinite half-space of conductive media on which the coil is lying. Because the implanted coil is located within the conductive media, $R_i$ can be approximated with twice the calculated value from Eq. [23]. The value of $m$ can be approximated with the free space formula for $B_1/Ip$ at $v$, or equivalently, $B_1/I_s$ at $v$, because the radii of the two coils are assumed to be the same:

$$m \cong \frac{B_1}{I_s}\pi b_i^2 \cong \frac{\mu_0 b_s^2}{2(b_s^2 + D^2)^{3/2}}\pi b_i^2. \qquad [24]$$

Therefore,

$$\frac{\mathrm{SNR}_p}{\mathrm{SNR}_s} \cong \left[\frac{(b_s^2 + D^2)^3}{2^3 b_s b_i^5}\right]^{1/2}. \qquad [25]$$

This formula provides the SNR advantage of surgically implanted, inductively coupled coils over surface coils and depends only on the geometry, i.e., the respective coil radii and the depth of the voxel of interest.

## EXPERIMENTAL RESULTS AND DISCUSSION

Although Eq. [25] can be calculated using simple geometric quantities, the more general Eq. [18] requires the calculation of the effective resistance through which power dissipates in a coil, i.e., $R_{\mathrm{coil}}$. Appendix A discusses the formulas used to calculate the three components of $R_{\mathrm{coil}}$:$R_{\mathrm{component}}$, $R_{\mathrm{sample}}$, and $R_{\mathrm{radiation}}$. To investigate the accuracy of the expressions for $R_{\mathrm{component}}$ and $R_{\mathrm{radiation}}$, the unloaded $Q$, or quality, factor of several single-turn resonant loops was measured, using an HP4195A vector impedance meter (Hewlett Packard, Inc., Boulder, CO). These data are plotted in Fig. 2 against

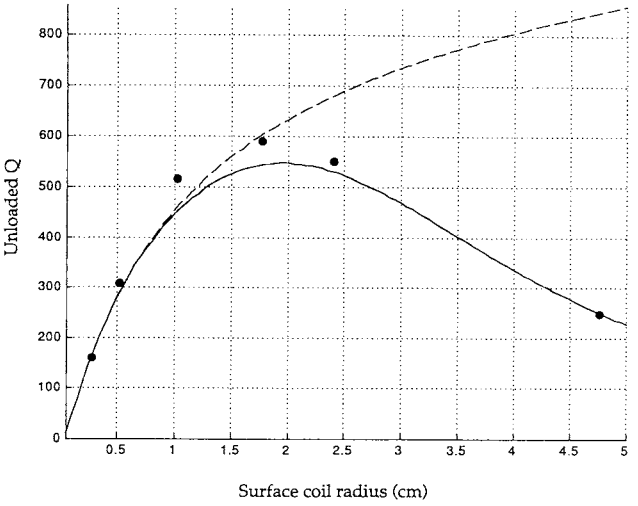


FIG. 2. Coil Q with (solid) and without (dashed) the inclusion of radiation losses. The circles represent measured values.

the calculated $Q$ according to the following formula

$$Q_{\mathrm{unloaded}} = \frac{\omega_0 L}{R_{\mathrm{component}} + R_{\mathrm{radiation}}}, \qquad [26]$$

where $L$ is the self-inductance of the coil. The dashed line in Fig. 2 shows the behavior in the absence of radiation resistance. These coils were constructed to be resonant at 300 MHz, proton Larmor frequency at 7 T. All results in this section are presented for this frequency. The $Q$ of the same coils was then measured with the coils lying against the surface of a large volume of 0.04 $M$ saline (~0.4 $\Omega^{-1}\mathrm{m}^{-1}$) (14) to investigate tissue loading. In Fig. 3 these data are plotted against the theoretical results calculated, assuming only inductive loading. Note that the empirical data corresponding to the largest coil in Fig. 2 is not plotted, because the loaded $Q$ was so low that it was difficult to measure. The difference between the theoretical and empirical results is assumed to be due to dielectric loading and some uncertainty about the effective coil radius (15).

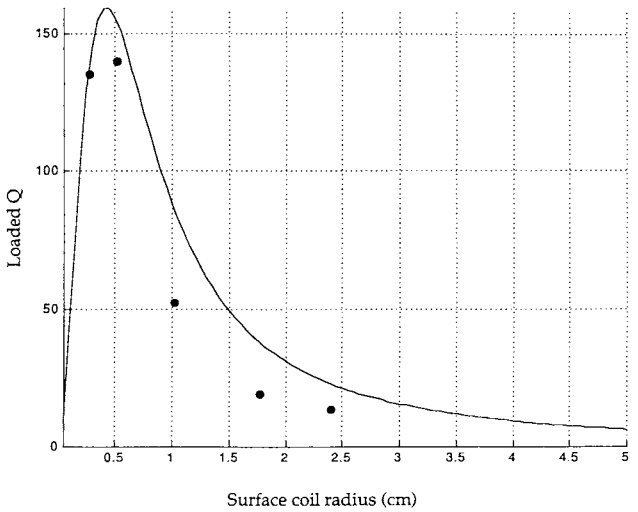


FIG. 3. Predicted and experimental (circles) loading data.

An assumption used to derive Eq. [25] was that the optimal surface coil radius and pickup coil radius, with respect to SNR, are equivalent. In Fig. 4, the SNR available to the preamplifier is plotted according to Eqs. [16] and [17], using both an implanted coil and a surface coil, respectively. The voxel of interest is assumed to lie 1.0 cm below the surface of the sample; the implanted coil radius is assumed to be 3 mm; and the sample itself is assumed to be a cylinder of height 2.0 cm, radius 2.0 cm, and conductivity 0.4 $\Omega^{-1}m^{-1}$. The maximum SNR is indicated with a circle on both graphs. Not only are the corresponding coil radii very similar, but the SNR is seen to be relatively insensitive to pickup and surface coil radii over a wide range of coil radii. The assumption that optimal surface and pickup coil radii are the same appears to be justified.

To investigate the accuracy of Eqs. [18] and [25], a cylindrical phantom 32 mm in diameter and 22 mm high was constructed and filled with 8% (by weight) bovine gelatin and sodium chloride to yield a net concentration of 0.08 *M* saline (8 ms/cm conductivity). In one set of acquisitions, a 6.0-mm ID implanted coil coated with a layer of parafilm 0.2 mm thick was placed at a depth of 5.8 mm in a gel phantom. The parafilm served as an insulator and as a means of reducing dielectric loading. This implanted coil was then coupled, in turn, to three separate self-resonant coils that had different IDs: 27, 17, and 9.5 mm. In each case, the wire diameter was roughly 2 mm, and an adjustable capacitor was used to adjust the net frequency obtained in the presence of the implanted coil to the proton Larmor frequency (300.5 MHz). A nonresonant pickup loop with a series capacitor was then inductively coupled to the resonant coil on the surface of the gel phantom. The series capacitor was useful in setting an impedance minimum, as seen through the fixed-length coaxial cable to which it was attached. The lower of the two resonant peaks that appear when two self-resonant coils are coupled together was adjusted to the Larmor frequency. In situations in which the space between two resonant coils is selected for viewing, the choice of the lower mode is necessary, for it is associated with a symmetric $B_1$ field (flip angle) pattern. Here, the field of view was restricted to the region around the implanted coil, so either mode would have sufficed.

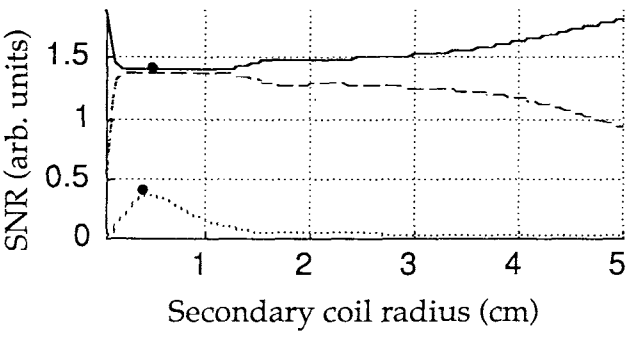


FIG. 4. Relative SNR values in the primary (solid line), the secondary coupled to the primary (dashed line), and a surface coil alone (dotted line). Note that the points of maximum SNR in the surface and secondary coils are nearly coincident (circles) in terms of coil radius.

Images perpendicular to the plane of the coil were acquired for the implanted coil coupled to each of the three surface coils. The power level was adjusted to achieve a 90° flip angle at the targeted voxel region (5 mm below the surface of the gel, centered on the implanted coil). For comparison, an identical gel phantom without the implanted coil was imaged with each of the three self-resonant coils now acting as surface coils. Again, the power level was adjusted to achieve a 90° flip angle for a voxel at a 5-mm depth with respect to the gel surface.

A conventional spin warp pulse sequence was used with $TE$ = 10 ms, $TR$ = 0.5 s, and a 50-KHz bandwidth. Sagittal sections (256 × 256 points) were acquired with a slice thickness of 1 mm. Image SNRs at the target voxel depth were calculated with a viewing program that calculates mean pixel intensities over a defined region of interest. Complementary noise values were measured in regions devoid of signal. Individual SNR measurements for the three implanted coil cases and the three corresponding surface coil cases were thus accomplished and are shown in Table 1.

As expected, there was no real dependence of implanted coil SNR on pickup coil size over the range used. Clearly, as the pickup coil becomes very small or very large, this will break down; however, an investigator would not have to worry about choosing the optimal coupling coil diameter. The flip angle patterns around the implanted coil did appear slightly different for the 9.5-mm coil and, thus, the SNR measurement was somewhat more uncertain. The data from Table 1 are plotted in Fig. 5, so as to check the accuracy of the model developed above. It is clear that the data are in reasonable agreement with the prediction and that the simplified formula derived in Eq. [25] is a very good predictor of the actual SNR advantage of implanted coils over that of surface coils for the range of coil sizes and implantation depths considered.

The divergence of the simplified formula in Fig. 5 is most likely due to finite size effects of the cylindrical phantom that were not taken into account in Eq. [25]. The radius of the cylinder, 1.6 cm, corresponds well to the radius in Fig. 5, at which the divergence becomes pronounced. Dealing with a large range of coil sizes (especially for subcentimeter-diameter coils) to explore a greater range in the experimental tests of the fit was difficult, but again, the agreement seems good.

Figure 6 shows the ratio of the SNRs for implanted and surface coils as a function of voxel depth for an implanted coil diameter of 7 mm and a surface/pickup coil diameter of 2 cm, assuming that the sample is an infinite half-space. It is clear that dramatic improvements are possible as the implanted coil depth increases. Of course, the image SNR obtained when using the implanted coil

Table 1
Measured Image SNR

| Coupling/surface coil size (mm) | Implanted coil | No implanted coil |
|---|---|---|
| 27 | 49–52 | 4.1–4.4 |
| 17 | 49–53 | 6.3–7.0 |
| 9.5 | 49–54 | 9.6–11 |

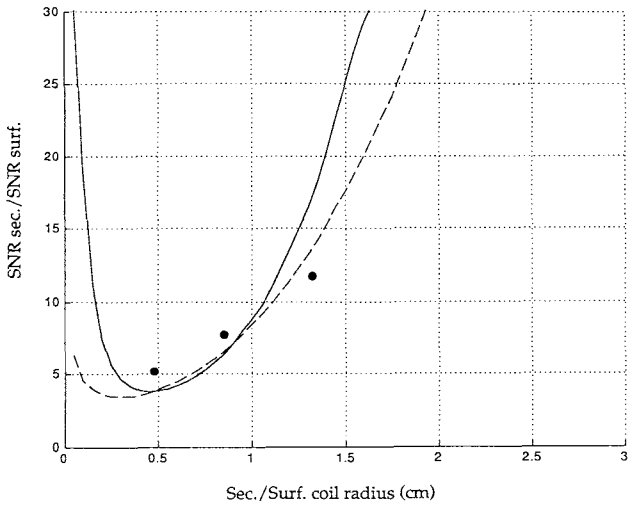


FIG. 5. Relative SNR improvement of an implanted coil, compared to that of a surface coil. The dashed line is the approximation given in Eq. [25]. The solid line is the more accurate approximation, given in Eq. [18]. The circles represent empirical data.

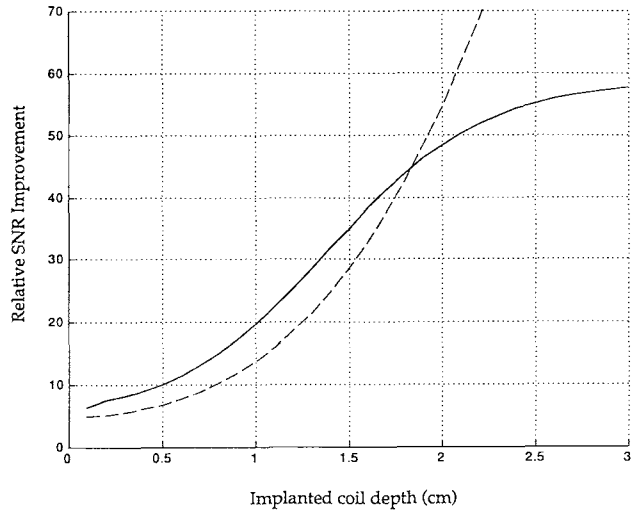


FIG. 6. Dependence of SNR improvement on voxel depth. The solid line is from Eq. [18], and the dashed line is the approximation, given in Eq. [25].

will still drop off with depth. A minimum image quality must be maintained, and this value can be estimated from our model. Again, we find that the agreement between Eqs. [25] and [18] is quite good over a wide range of coil depths.

## CONCLUSION

An expression for the SNR advantage of a surgically implanted imaging coil over a surface coil for *in vivo* imaging has been derived and empirically verified. An even simpler expression involving only coil radii and the depth of the voxel of interest has also been derived and has been shown to be empirically valid, assuming that the resistance of the implanted coil referred to the pickup coil is much greater than the nominal pickup coil resistance (i.e., $R_i \rightarrow \rho \gg R_p$). It is seen that this simplified expression holds over a large range of practical situations and thus provides the investigator with a useful tool in assessing the advantages of implanted coils for a given set of geometric conditions.

This discussion has been restricted to an operating frequency of 300 MHz, although a similar analysis at any practical operating frequency should be straightforward, using the formulas presented.

## APPENDIX A

The component resistance consists of conductor resistance $R_{\text{cond}}$ and the effective series resistance (due to dielectric loss) of the chip capacitor that is typically used to construct the resonant coil, $R_{\text{cap}}$. The resistance of any coil solder joints is neglected.

$$R_{\text{cond}} = \frac{l\rho}{A} = \frac{a\rho}{r\delta} = \frac{a\rho}{r}\left[\frac{2\rho}{\mu\mu_0\omega_0}\right]^{-1/2}, \qquad \text{[A1,A2]}$$

$$= \frac{a}{r}\left[\frac{\mu_0\omega_0\rho}{2}\right]^{1/2}$$

where $a$ is the coil radius, $l$ is the circumference of the coil, $\rho$ is the resistivity of the conductor (taken to be that of Cu $1.77 \cdot 10^{-8}$ $\Omega$m), $A$ is the effective cross-section of the conductor through which current flows, $r$ is the radius of the wire conductor, taken to be $3.2194 \cdot 10^{-4}$m (the radius of 22-gauge wire), $\delta$ is the skin depth, $\mu$ is the relative permeability of the conductor, taken to be that of copper, $\approx 1.0$, $\mu_0$ is the permeability of free space, and $\omega_0$ is the Larmor frequency corresponding to $B_0$. $R_{\text{cap}}$ can be determined from the manufacturer's data. $R_{\text{cap}} = (\omega_0 CQ)^{-1}$, where $C$ is the capacitance value and $Q$ is the quality factor of the capacitor.

For high $Q$ capacitors, the $CQ$ product is approximately $10^{-8}$ at 300 MHz and $10^{-7}$ at 65 MHz. At these frequencies, $R_{\text{cap}}$ is, therefore, approximately 0.05 and 0.02 $\Omega$, respectively. $R_{\text{sample}}$ can be determined by integrating the square of the coil vector potential over the space of the specimen (8):

$$R_{\text{sample}} \cong g\omega_0^2 \int_{\text{sample}} |A/I|^2 \, dv, \qquad \text{[A3]}$$

where $g$ is the sample conductivity.

A formula for **A**, taking into account skin depth effects or eddy current shielding, is provided by Hammond (9), assuming that the specimen is uniform and fills a half-space below the plane of the coil.

When the radius of the circular coil is small, compared with that of the antenna wavelength, $R_{\text{radiation}}$ is given by Terman (2) as

$$R_{\text{radiation}} \cong 31{,}200(a/\lambda^2)^2, \qquad \text{[A4]}$$

where $a$ is the coil radius and $\lambda$ is the wavelength associated with $\omega_0$.

## ACKNOWLEDGMENTS

The authors thank G. A. Johnson for intellectual support and Elaine G. Fitzsimons for editorial assistance.

## REFERENCES

1. J. F. Schenck, H. R. Hart, T. H. Foster, W. A. Edelstein, M. A. Hussain, High resolution magnetic resonance imaging using surface coils, *in* "Magnetic Resonance Annual 1986" (H. Kressel, Ed.), pp. 123–160, Raven Press, New York, 1986.
2. F. E. Terman, "Radio Engineer's Handbook," McGraw-Hill, New York, 1943.
3. X. Zhou, R. R. Maronpot, G. P. Cofer, L. W. Hedlund, G. A. Johnson, Studies on bromobenzene-induced hepatotoxicity using *in vivo* MR microscopy with surgically implanted rf coils. *Magn. Reson. Med.* **31,** 619–627 (1994).
4. M. D. Schnall, C. Barlow, V. H. Subramanian, J. S. Leigh, Wireless implanted magnetic resonance probes for *in vivo* NMR. *J. Magn. Reson.* **68,** 161–167 (1986).
5. J. C. Ford, D. B. Hackney, P. M. Joseph, M. Phelan, D. C. Alsop, S. L. Tabor, C. M. Hand, R. S. Markowitz, P. Black, A method for *in vivo* high resolution MRI of rat spinal cord injury. *Magn. Reson. Med.* **31,** 218–223 (1994).
6. T. H. R. Farmer, G. P. Cofer, G. A. Johnson, Maximizing contrast to noise with inductively coupled implanted coils. *Invest. Radiol.* **25,** 552–558 (1990).
7. L. L. Arnder, X. Zhou, G. P. Cofer, L. W. Hedlund, G. A. Johnson, Magnetic resonance microscopy of the rat carotid artery at 300 megahertz. *Invest. Radiol.* **29,** 822–826 (1994).
8. M. D. Harpen, Sample noise with circular surface coils. *Med. Phys.* **14,** 616–618 (1987).
9. P. Hammond, The calculation of the magnetic field of rotating machines. Part 3. Eddy currents induced in a solid slab by a circular current loop, *in* "Proc., IEEE (monograph 514S) 109C," pp. 508–515, 1962.
10. K. E. Ekstrand, R. L. Dixon, Electricity and magnetism for NMR: a review of basic concepts, *in* "NMR Medicine: The Instrumentation and Clinical Applications" (S. R. Thomas, R. L. Dixon, Eds.), Medical Physics Monograph 14, American Association of Physics in Medicine (American Institute of Physics), New York, 1986.
11. D. I. Hoult, P. C. Lauterbur, The sensitivity of the zeugmatographic experiment involving human samples. *J. Magn. Reson.* **34,** 425–433 (1979).
12. D. I. Hoult, R. E. Richards, The signal-to-noise ratio of the nuclear magnetic resonance experiment. *J. Magn. Reson.* **24,** 71–85 (1976).
13. W. R. Symthe, "Static and Dynamic Electricity," 3rd ed., McGraw-Hill, New York, 1968.
14. T. W. Redpath, J. M. S. Hutchinson, Estimating patient dielectric losses in NMR images. *Magn. Reson. Imaging* **2,** 295–300 (1984).
15. M. B. Banson, G. P. Cofer, R. D. Black, G. A. Johnson, A probe for specimen magnetic resonance microscopy. *Invest. Radiol.* **27,** 157 (1992).